Testing Models of Ultra-Fast India-Asia Convergence: New Paleomagnetic Results from Ladakh, Western Himalaya

by

Elizabeth A. Bailey

Submitted to the Department of Earth, Atmospheric and Planetary Sciences

in Partial Fulfillment of the Requirement for the Degree of Bachelor of Science

at the Massachusetts Institute of Technology

May 12, 2014
[June 2014]

Signature redacted

Author_____
Elizabeth Bailey
Department of Earth, Atmospheric and Planetary Sciences
April 16, 2013

Signature redacted

Certified by_____
Benjamin P. Weiss
Thesis Supervisor

Signature redacted

Accepted by_____
Richard P. Binzel
Chair, Committee on Undergraduate Program

Abstract

Rapid India-Asia convergence has led to a major continental collision and formation of the Himalayas, the highest mountain range on Earth. Knowledge of the paleolatitude of the Kohistan-Ladakh Arc (KLA), an intermediate tectonic unit currently situated between the converging Indian and Eurasian continents in Western Himalaya, would constrain the tectonic history and dynamics of Himalayan orogenesis. We present new paleomagnetic data from the Khardung volcanic rocks of the Shyok-Nubra valley region of Ladakh, western Himalaya. Samples from all four sites (KP1-KP4) display high-temperature components indicating a roughly equatorial paleolatitude, with the average of site mean directions implying a paleolatitude of 5°N. We interpret results of a positive baked contact test at one site (KP3) to imply that the high-temperature components in the distal volcanic bedrock predate bedding tilt and dike formation. Previous studies of the Khardung unit (Bhutani 2009, Dunlap 2002) have measured ^{40}Ar-^{39}Ar and U-Pb dates of ~52-67 Ma. Assuming these ages apply to our samples, our results support the two-stage collision model of Jagoutz and Royden (in prep), which indicates an approximately equatorial India-KLA collision at 50 Ma.

Acknowledgements

First I want to thank Professor Ben Weiss for advising me on this project and for being an indispensable source of advice and encouragement in the past year. I also want to thank Profs. Leigh Royden and Oliver Jagoutz for useful discussions.

Additional gratitude is directed to Dr. Sonia Tikoo for all the time and help she has provided, as well as the other people of the MIT Paleomagnetism Laboratory for their advice and patience, without which this work wouldn't have been possible. Furthermore, graduate students Ben Klein and Claire Bucholz have provided helpful ideas and field notes, as well as labeled photographs of our field sites.

Special thanks go to Dorjay, our guide on the field trip, for his bravery in getting me medical treatment when I developed severe altitude sickness in the night at Sarchu, as well as to his family for their kindness and hospitality during our trip.

Finally, I thank my parents, as well as all my colleagues, mentors, and friends both inside and outside the department, for helping me develop as a scientist and person, and for generally being nice to have around.

1.0 Introduction

The convergence of India and Eurasia due to divergence of India from the southern supercontinent Gondwana at ~120 Ma (Gaina et al. 2007, van Hinsbergen et al. 2011) has resulted in a great collision, giving rise to the Himalayas. A ~400 mile arc reaching from present-day Afghanistan to the Sichuan and Yunnan provinces of China, this mountain region comprises the largest and youngest known orogenic system (Yin and Harrison 2000, Keary et al. 2009, Molnar 1984, Yin and Harrison 2000).

Because the Himalayan region is a prominent topographic feature and the largest known reservoir of water ice outside the polar regions (Owen et al., 2002), these mountains have played a significant role in shaping local climate patterns, such as the Indian and South Asian monsoons and the mid-Westerlies (Yin and Harrison 2000, Owen 2002). The Himalayas are postulated to have a significant effect on global-scale climate, sea level, and ocean chemistry (Molnar and England 1990, Raymo 1994, Rea 1992). Mechanisms have been suggested in which climate influences tectonic behavior (Allen and Armstrong 2012, Beaumont et al. 1992, Molnar and England 1990), indicating the existence of feedback loops between climate and tectonics. Furthermore, the resultant closure of the ocean between India and Eurasia has influenced global oceanic circulation (Yin and Harrison 2000, Khan 2009).

Thus, the outstanding size of the Himalayan orogen led to its significant role not only in Earth's lithosphere, but also the atmosphere, hydrosphere, and cryosphere. The high rate of India-Eurasia convergence (Molnar and Tapponnier 1975) that resulted in this great size raises questions about the manner of plate movement. Established tectonic models indicate that from 65-50 Ma, the India-Eurasia convergence attained speeds of

130-180 mm/yr, nearly double the fastest known present-day subduction rates (Jagoutz and Royden in prep, Cande 2010, van Hinsbergen et al. 2012, Müller et al. 2008, Capitanio et al. 2010).

Several models have been proposed to explain rapid India-Asia convergence. Some models assume a single subduction zone between India and Eurasia and account for the unusually fast subduction with various explanations (Capitanio et al. 2010). The presence of a plume head beneath the Indian plate has also been suggested to have driven India's rapid motion (Kumar et al. 2007, Cande and Stegman 2011). Based on numerical simulations, van Hinsbergen et al. (2011) argue that lateral asthenospheric motion associated with presence of a plume head is insufficient by itself to account for convergence rates at 65-50 Ma. Other models include multiple subduction zones between India and Eurasia, including models with a continental plate (van Hinsbergen et al. 2012) or an oceanic plate (Jagoutz and Royden 2013, in press) occupying the region between subduction zones.

The Himalayan orogen includes a complex amalgamation of material exposed between the established boundaries of the Eurasian and Indian plates (Kearey et al. 2009, Bouihol et al. 2013). By virtue of its intermediate location between India and Eurasia, an understanding of past locations of this material can offer insight into the dynamics of India-Eurasia convergence. Because paleomagnetic analysis gives the paleolatitude of samples, and because relative motion between India and Eurasia occurred in a primarily north-south direction, paleomagnetism can provide powerful tests that could distinguish between the above models.

We present new paleomagnetic results from samples of the Khardung volcanic rocks, which overlie the Kohistan-Ladakh Arc (KLA). Today, the KLA lies between India and Eurasia and is interpreted to have been an island arc situated in an ancient ocean between the two continents (Bouihol et al. 2013, Jagoutz and Royden in prep). Our results indicate that Ladakh occupied an approximately equatorial position when the northern extent of India collided with the KLA, which we tentatively constrain to have occurred at ~67-52 Ma based on previous radiometric dating of other samples from the Khardung volcanics (Dunlap 2002, Bhutani 2009). Although radiometric dating of our own samples is necessary, this result appears to be in agreement with the two-stage collision model of Jagoutz and Royden (2013 in prep).

We proceed with the discussion as follows: Section 1 includes a brief description of Himalayan geological context, an overview of current understanding of the paleolocations of India, Eurasia, and the KLA, an overview of existing models to account for rapid India-Eurasia convergence, and an overview of the field site. Section 2 describes our methods for sample collection and paleomagnetic analysis. The results of this analysis are presented in Section 3, followed by discussions and implications of this work in Sections 4 and 5.

1.1 Overview of Himalayan Geology

We review current understanding and classification of large-scale Himalayan tectonic structure (Figure 1). The Karakoram and Gangdese Batholiths comprise the southern margin of Eurasia. The KLA is trapped between Eurasia and India, north of the western extent of the Himalayan belt. The Tsangpo, Indus, and Shyok suture zones separate these units (Kearey et al. 2009, Bouihol et al. 2013, Jagoutz and Royden 2013, in prep).

The KLA is comprised of two lobes, Kohistan to the west and Ladakh to the east (Bouihol et al. 2013, Jagoutz and Royden 2013, in prep). The KLA is bounded to the south by the Indus Suture Zone, and to the north by the Shyok Suture Zone (SSZ). The location of the SSZ is interpreted to consist of ophiolitic mélange extending along the northern boundary of the KLA (Dunlop 2003). The Karakoram Fault, reaching across the northeastern boundary of Ladakh, comprises the eastern extent of the SSZ. The Karakoram fault also marks the boundary between the Gangdese batholith to the east and the Karakoram batholith to the west (Figure 1).

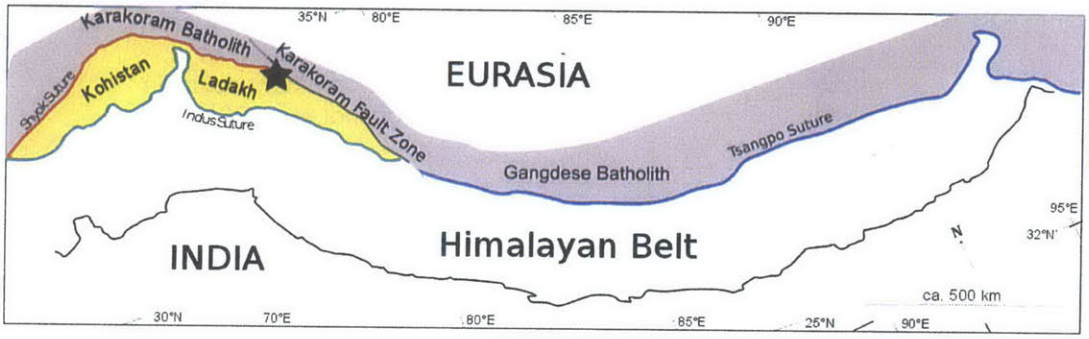

Figure 1: Map of large-scale Himalayan tectonic structure. Figure adapted from Royden and Jagoutz (in prep). The grey region indicates the Karakoram and Gangdese Batholiths; yellow indicates the KLA. The black star marks the location of our field site.

1.2 Established motions of India, Eurasia, and the Kohistan-Ladakh Arc

At a latitude of ~70°E, Eurasia has remained at ~25-30°N since 130 Ma (van Hinsbergen et al. 2012, Jagoutz and Royden in prep). The Indian plate has experienced northward motion of ~60°N since 120 Ma (Figure 2), including several accelerations or decelerations relative to Eurasia: notably, a rapid decrease in convergence rate from

~130-180 mm/yr to ~50 mm/yr from ~50-35 Ma, as well as increases in convergence rate at ~65-50 Ma and ~90 Ma (Yin and Harrison 2000, van Hinsbergen et al. 2011, Jagoutz and Royden in prep). The decrease in convergence rate beginning at ~50 Ma has commonly been attributed to the final India-Eurasia collision (Zhu 2005). However, recent results (Bouilhol et al., 2013) have dated the India-Eurasia collision at 40 Ma.

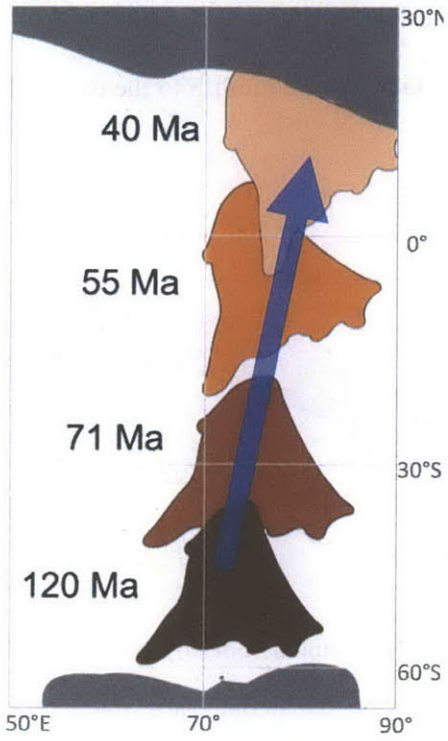

Figure 2: Northward motion of India toward Asia from 120 Ma (Molnar and Tapponnier 1975, Bouilhol et al. 2013). Rapid India-Asia convergence of 130-180 mm/yr occurs at ~65-50 Ma, while slowdown to ~50 mm/yr occurs between 50-35 Ma (Jagoutz and Royden, in prep, van Hinsbergen et al., 2012). Final continent-continent collision occurs at 40 Ma (Bouilhol et al. 2013).

Paleomagnetic work has previously been carried out to constrain the paleolatitude of the KLA (e.g., Molnar and Tapponnier 1975). Klootwijk et al. (1979) determined a paleolatitude of 7-10°N of samples of the Ladakh intrusives at Kargil, which formed at 49-45 Ma. Khan et al. (2009) have presented evidence, based in part on paleomagnetic work on the Utror Formation near the KLA's southern margin, that India and the KLA collided near the equator at ~65 Ma. Our study site (Sections 1.4, 2.1) consists of the Khardung volcanics in the Shyok-Nubra valley at the northeastern extent of Ladakh.

1.3 Prior models of rapid India-Asia convergence

Various models have been proposed to explain rapid India-Asia convergence. We note two unexplained features of the relative motion between India and Eurasia. First, the decrease in convergence rate at 50 Ma is less abrupt than collisions for other known orogens (Royden and Jagoutz in prep, Capitanio et al. 2010). The second notable feature of convergence is the spectacular rate of 130-180 mm/yr observed from 65-50 Ma (Royden and Jagoutz in prep, van Hinsbergen et al. 2011).

Capitanio et al. (2010) propose that the Indian continent was dense and thus easily subducted beneath Eurasia after collision, accounting for gradual slowdown after 50 Ma. Kumar (2007) and van Hinsbergen et al. (2011) argue that presence of the Reunion plume head beneath India enhanced the mobility of India and can account for the rapid convergence rates from 65-50 Ma.

The models mentioned above assume a single subduction zone between India and Eurasia. Royden and Jagoutz (in prep) argue that models proposing single subduction zones between India and Eurasia fail to account for ultra-fast convergence at 65-50 Ma, and have presented the following model: two north-dipping subduction zones extended across the entire east-west extent of the Indian-Eurasian boundary, with an oceanic plate between the two continental plates (Figure 3, top). At 50 Ma, the northern extent of India experienced a collision with an island arc system, comprised at least in part by the KLA, at a roughly equatorial position. The result of Bouilhol et al. (2013) that final India-Eurasia closure occurred at 40 Ma rather than the previously assumed 50 Ma supports the possibility that India's deceleration at 50 Ma was due not to its contact with Eurasia, but rather to this arc-continent collision. Finally, this model ascribes the non-abrupt

slowdown of convergence after 50 Ma to the continued subduction of oceanic plate beneath Eurasia. Jagoutz and Royden (in prep) thus offer an explanation for both the rapid convergence at 65-50 Ma and gradual slowdown starting at 50 Ma.

Another two-stage collision model has been proposed by van Hinsbergen et al. (2012). In this model, a microcontinent exists between India and Asia which first collides with the southern boundary of Eurasia at 50 Ma, at a latitude of ~25-30°N. Then, a final continent-continent collision of India against the southern boundary of the microcontinent occurs at ~23 Ma.

Jagoutz and Royden (in prep) and van Hinsbergen et al. (2012) both propose that there were two collisions during the convergence of India and Eurasia. The collisions in these models differ, however, in the timing, position, and proposed land masses involved. According to van Hinsbergen et al., the first collision occurred at 50 Ma when an intervening microcontinent collided with the southern extent of Eurasia at a latitude of ~25-30°N. Alternatively, according to Jagoutz and Royden, the first collision occurred between the KLA and the northern extent of India at a roughly equatorial latitude. In van Hinsbergen et al.'s double-collision model, the KLA was already located at ~25°N by 60 Ma, while in Jagoutz and Royden's model, the location of the KLA was roughly equatorial until India collided with it and dragged it northward at ~50 Ma, until the final collision at ~40 Ma.

The model of van Hinsbergen et al. (2012) implies that samples from the KLA with an age of 60 Ma or younger would give inclinations of at least 40°, corresponding to a paleolatitude of 23°N. Jagoutz and Royden's model (2013) implies that samples with an

age of 50 Ma or older would instead give inclinations of no greater than 0-36°, corresponding to a paleolatitude of 0-20°N.

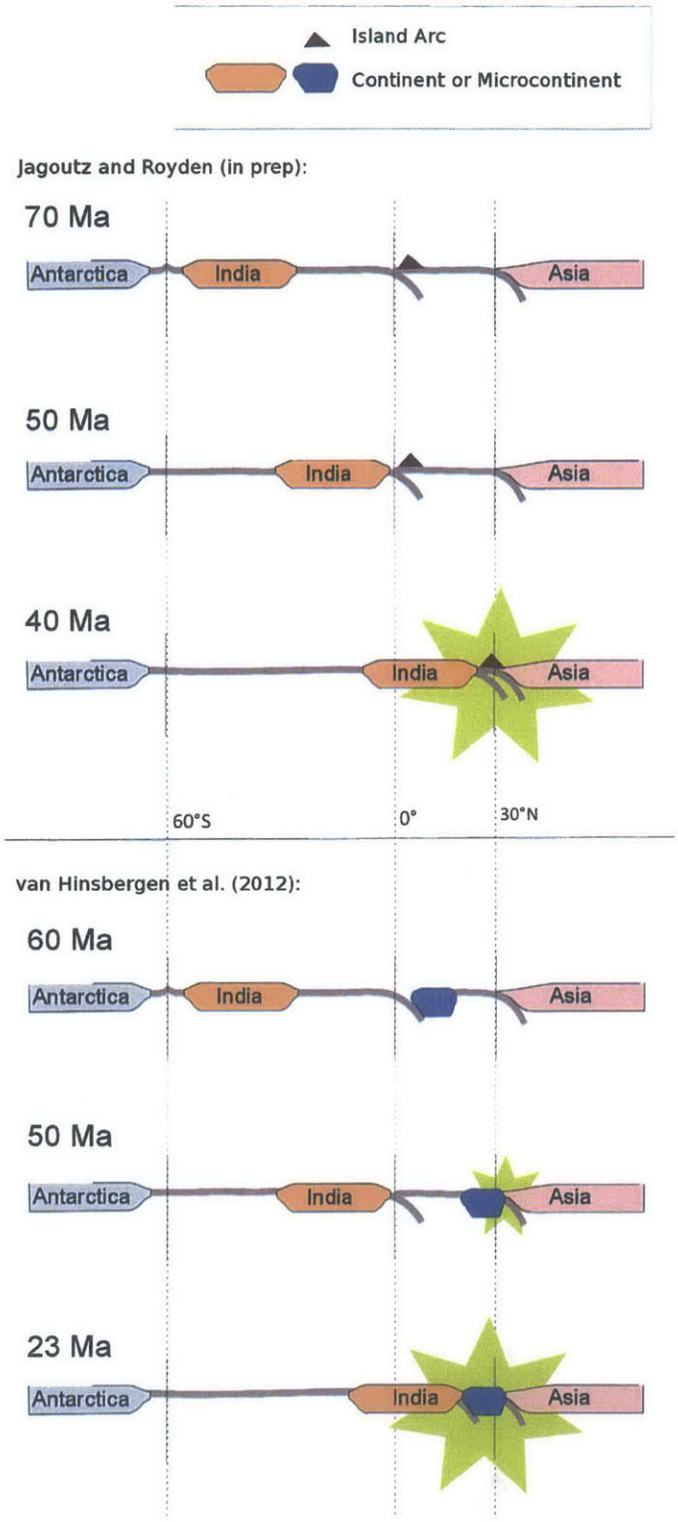

Figure 3: Horizontal transects depicting the two-stage collision models of Jagoutz and Royden (in prep) and van Hinsbergen et al. (2012). Transects represent the north-south extent between Antarctica and Asia, with a longitude of approximately 75°E.

Top: Jagoutz and Royden (in prep) have the first collision occurring between India and the intervening material at 50 Ma, followed by final continent-continent convergence at 40 Ma. Note roughly equatorial position of intervening material at 50 Ma.
Bottom: van Hinsbergen et al. have the first collision as a microcontinent-continent collision at the southern boundary of Asia at 50 Ma, followed by the final continent-continent collision at ~23 Ma.

1.4 Regional geographic context

The Shyok and Nubra Rivers are taken to mark the approximate location of the Karakoram Fault in the study area (Figure B-1), with their confluence occurring near the villages of Diskit and Tirit. Zones of ophiolitic mélange extend along the vicinity of the Karakoram Fault in this region (Bhutani et al. 2003). Volcano-sedimentary material is deposited along the SSZ between the Karakoram Batholith in the north and the Ladakh Batholith in the south (Bhutani et al. 2009, Bhutani et al. 2003, Dunlap and Wysoczanski 2002). These materials have been grouped into two categories: the Shyok Volcanics and the Khardung Volcanics (Bhutani et al. 2003).

The Shyok Volcanics consist primarily of basalt, basaltic andesite, and andesite exposed near the Nubra and Shyok rivers (Bhutani et al. 2009). The Khardung volcanics comprise our sampling locations (Appendix B, Figure B-1). Deposited near their namesake village southwest of the Shyok River, the Khardung volcanics are a ~500 m thick dome overlying the Ladakh batholith (Bhutani et al. 2003, Bhutani et al. 2009). Classified as felsic or acidic (Bhutani 2003, Dunlap 2002) and calc-alkaline (Srimal 1986), they include rhyolite and pyroclastics (Bhutani 2003, Dunlap 2002) with a minority of andesite and basalt (Thakur and Misra 1984). Compared to the Shyok volcanics, with which they are in tectonic contact, the Khardung volcanics are undeformed and comparatively unaffected by recent heating events that might affect apparent ^{40}Ar-^{39}Ar age spectra, with which they are in tectonic contact (Bhutani et al. 2009).

Prior work has been done to date the Khardung volcanics. Sharma (1978) determined an age of ~38 Ma, but these dates were based on K-Ar and ^{40}Ar-^{39}Ar methods, which Dunlap and Wysoczanski (2002) argued were unreliable. Dunlap and Wysoczanski (2002) used U-Pb dates to constrain the age of one section to ~67.4-60.5 Ma. Based on ^{40}Ar-^{39}Ar dates of rhyolite samples (Figure B1), Bhutani et al. (2009) have estimated a minimum emplacement age of ~52 Ma for the Khardung volcanics.

2.0 Methods

2.1 Sample Collection

During one field trip in August 2013, samples were acquired from 4 sites in the Khardung volcanics (KP1-KP4) along a road cut (Appendix B).

Oriented samples of rhyolite and volcaniclastics were collected from sites KP1, KP2, KP3, and KP4. Based on the northward bedding tilt and the north-south arrangement of samples (Figure B1), from youngest to oldest, the samples are likely to be ordered as: KP4, KP1, KP2, KP3. Core samples were drilled from the host rock using handheld drills with water-cooled, diamond-tipped bits. Block samples were collected with nonmagnetic hammers and chisels. Core and block samples were oriented before their removal from the host rock.

A rhyolitic dike ~5 m wide was found to have intruded at site KP3. The presence of this dike allowed for a baked contact test at site KP3. Hence, the distance from sample locations to the exposed area of dike was recorded.

In total, 37 cores with diameter ~2.5 cm were collected from the sites (8 cores at site KP1, 9 cores at KP2, 12 cores at KP3, and 8 cores at KP4). An additional 3 oriented cores were extracted from the KP3 dike block samples using a drill press with bit similar

to that used in the field. A total of 87 oriented samples, each ~1 cm thick, were sliced from the 40 cores using a rotating diamond saw, with each core yielding 1-5 samples.

2.2 Paleomagnetic analysis

All samples were analyzed in three stages:

1) The natural remanent magnetization (NRM) was measured.
2) Stepwise alternating field (AF) demagnetization was performed in 1 mT steps to 10 mT, and remanent magnetization measured after each AF step.
3) Stepwise thermal demagnetization was performed on the samples in steps from 50° to 660°C (50°C steps from 50° to 200°, 25°C steps from 225° to 550°, then 5° to 25° steps thereafter), and remanent magnetization was measured after each heating step.

All measurements were performed at the MIT Paleomagnetism Laboratory with a 2G Enterprises Superconducting Rock Magnetometer. AF demagnetization steps were carried out with an in-line automatic sample degaussing system. Stepwise heating was performed in an ASC Scientific Model TD-48SC Thermal Specimen Demagnetizer (oven). The magnetometer and thermal demagnetizer were housed in an IMEDCO AG shielded room (MSR) rated to achieve >20 dB attenuation at frequency 1 Hz. The ambient field intensity of the oven has been reported at <10 nT (Bradley 2013).

Samples were considered demagnetized (i.e. were no longer considered to be carrying the primary remanence) when, at successive thermal steps, the magnitude of their moments no longer walked monotonically toward the origin and magnetization directions vacillated wildly.

Magnetization components were determined via principal component analysis (Kirschvink 1980) using the PaleoMag 3.1 software (Jones 2002). Linear least-squares fits were derived from components removed at AF steps or lower temperatures. Linear least-squares fits were also derived from high-temperature components that were clearly origin trending and hence interpreted to be the characteristic magnetization (ChRM) direction. In some cases, the final component appeared nonlinear or non-origin-trending. Interpreting such behavior to indicate incomplete demagnetization of a sample, in such cases we fit a circular arc to the final component.

For each site, the site mean direction was calculated via the application of Fisher statistics to the interpreted ChRM directions. Fisher statistics were also applied separately to the lower-temperature or lower-coercivity components at each site. For components having a reverse polarity compared to the majority of samples with which they were grouped, the reverse direction was considered (Jones 2002).

3.0 Results

Components of magnetization direction were classified for sites KP1 through KP4. Many samples exhibit multiple components, in which case we assign each component to one of two categories: (1) high-temperature (HT) components, which we take to be the primary components, and (2) lower-temperature or low-coercivity (LT) components, which we interpret to be secondary overprints, that were removed at AF or thermal steps prior to those that removed the HT component for each sample. For a minority of samples,

multiple magnetization components were not identified—in such cases, the single identified magnetization direction is grouped as an HT component.

Different samples varied in the temperatures at which magnetization components were removed. We interpret these differences in components as representing mineralogical differences between samples. Samples from all sites commonly exhibited components removed at steps between 560°C and 580°C, likely belonging to magnetite or maghemite. Some samples from site KP4 exhibited components not completely removed by 660°C, likely belonging to hematite. Many KP1 samples give LT components that are removed at steps before 150°C, possibly indicating the presence of goethite, which has a Néel temperature between 70°C and 125°C and (Tauxe 2010, after Dunlop and Özdemir 1997).

3.1 Site mean directions

Mean directions of the LT and HT components were computed separately for sites KP1, KP2, and KP4 (Figure 4, Figure A1, Table 1). At site KP3, the location of the baked contact test, mean directions (Figure 3, Table 2b) were calculated separately for:

(i) HT and LT components of dike magnetization

(ii) Components for baked samples (KP3-1 through KP3-4). See Table 2a for sample-dike distances. For each baked sample, a single component (HT) was identified.

(iii) HT and LT components for samples KP3-40 through KP3-45, which were all ~40-50 m away from the dike.

Table 1: Site mean directions for HT and LT components of samples from sites KP1, KP2, and KP4 in geographic and tilt-corrected coordinates. *N*=number of samples used to calculate Fisher mean direction, *D*: Declination of mean direction, degrees east of true north, *I*: Inclination of mean direction, positive down, α95: width of radius of 95% confidence circle of Fisher mean, *k*: Fisher precision parameter.

			Geographic coordinates			Tilt-corrected coordinates			
		N	*D* (°)	*I* (°)	α95 (°)	*D* (°)	*I* (°)	α95 (°)	*k*
HT	KP1	13	140.7	-40.4	15.8	170.9	-17.4	16.1	13
	KP2	20	150.3	-31.9	15.3	166.9	-5.9	15.4	20
	KP3	Site of baked contact test - see Table 2							
	KP4	25	161.8	-50.6	9.6	178.8	-6.5	9.6	23
LT	KP1	19	1.4	43.5	17.4	12.4	43.6	18.5	18
	KP2	29	353	52.2	11.1	13	9.4	11.1	33
	KP3	Site of baked contact test - see Table 2							
	KP4	31	353.8	46.5	7.8	3.9	-2.3	8.6	31

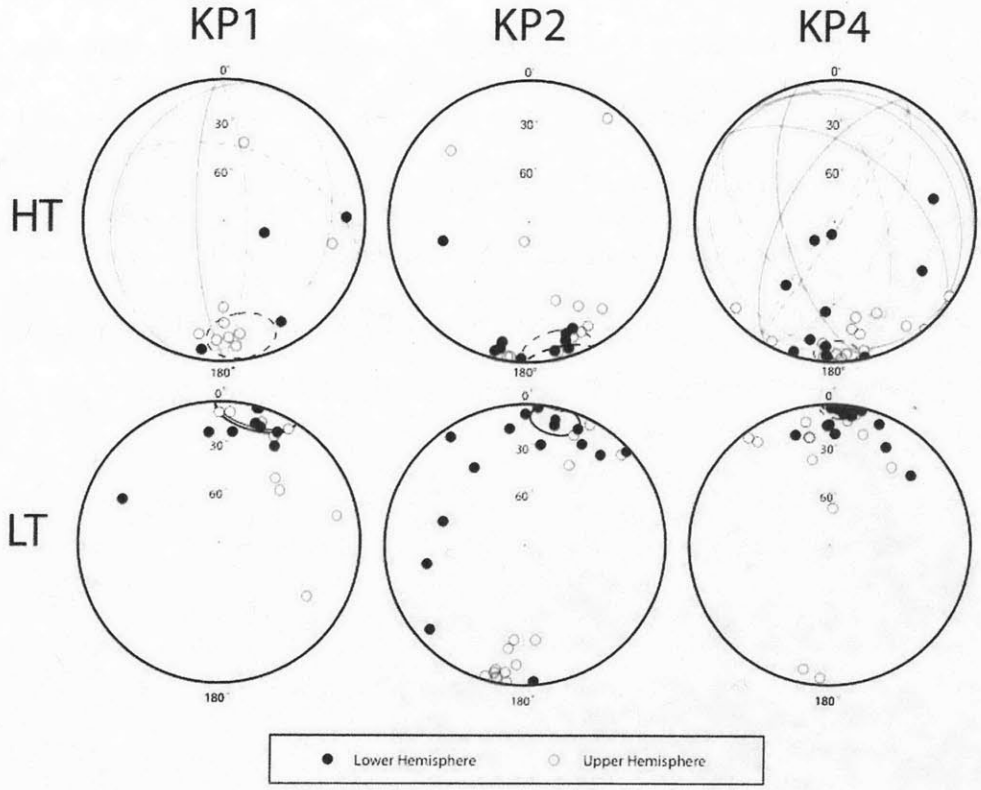

Figure 4: Site mean directions for high-temperature (HT) and Low-temperature (LT) components are shown in geographic (non-tilt-corrected) coordinates with stereographic plots for sites KP1, KP2, and KP4. Great circles represent best-fit arcs calculated with Fisher statistics, while small circles represent mean site directions, also calculated with Fisher statistics.

3.2 Results of the Baked Contact Test

We now discuss results of the baked contact test at site KP3. The dike at this site was ~5 m wide. Six samples from site KP3 (KP3-1 to KP3-6) were within 4 m of the dike. Five samples from site KP3 (KP3-40 to KP3-45) were ~40-50 m from the dike, at the road cut.

Samples from cores KP3-1 to KP3-4 all exhibited single magnetization components close to the HTd component of the dike samples (Figure 5a). We interpret this result to imply that cores KP3-1 to KP3-4 were completely thermally remagnetized during local heating from dike intrusion. Lack of scatter among baked sample directions, in contrast to the scatter seen among data from other samples, indicates a rapid thermal remagnetization event that did not record secular variation. Samples from KP3-5 to KP3-6 did not yield clear components of remanence and were thus excluded from this analysis. Samples at KP3 far from the dike (KP3-40 to KP3-45) displayed HT and LT components dissimilar to those of the dike and baked samples KP3-1 to KP3-4 (Figure 5[b-c]).

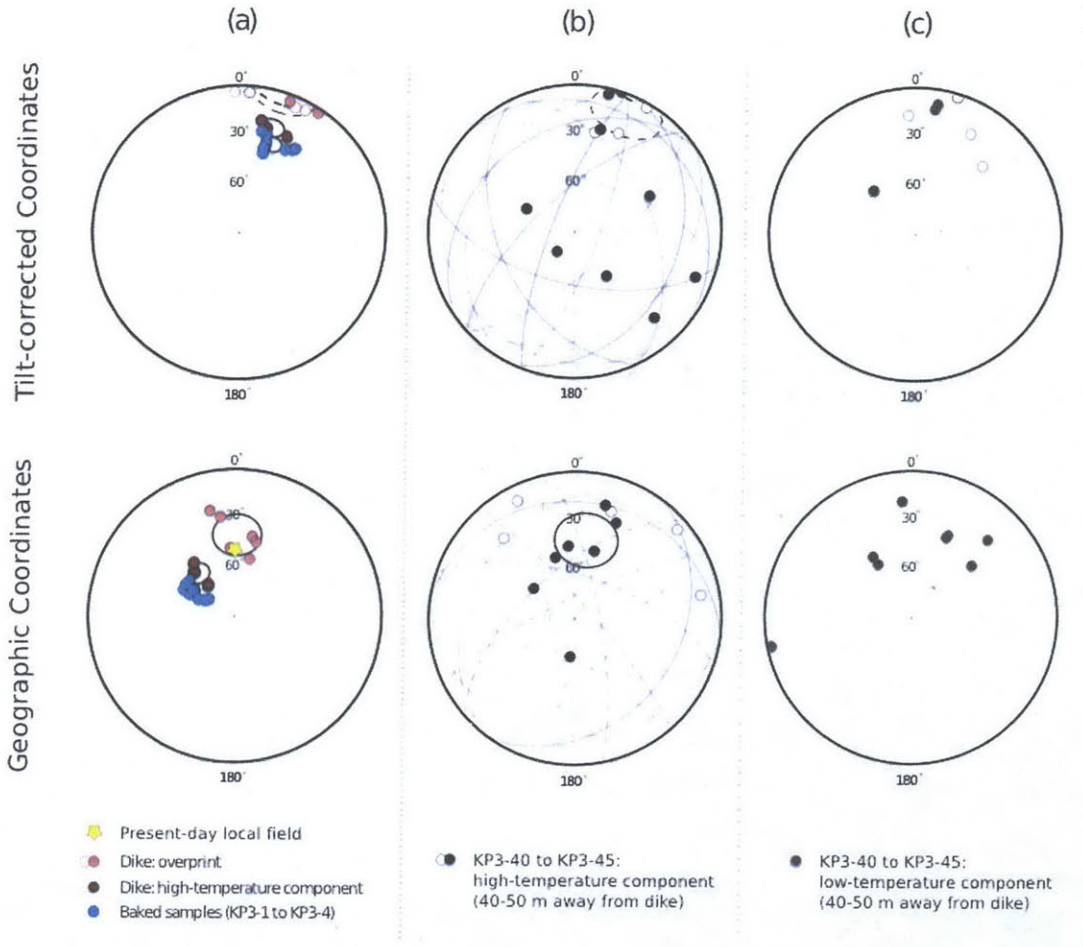

Figure 5: Stereographic plots showing results of the baked contact test, with and without tilt-correction. Mean Fisher directions of 5 categories of sample. Solid circles indicate points on the lower hemisphere and empty circles indicate points on the upper hemisphere. Column (a) shows high-temperature and low-temperature components of the dike and high-temperature components of baked samples. Column (b) shows the high-temperature components of samples located ~40-50 m from the dike, while column (c) shows the low-temperature components of those samples. Grey great circles in column (b) represent best-fit arcs of Fisher circle fits.

Tables 2(a-b): Results of the dike test. (a) Sample distances from dike. Dike width was ~5 m. (b) Site mean directions for HT and LT components of samples from site KP3. *N*: number of samples used to calculate Fisher mean direction, *D*: Declination of mean direction, degrees east of true north, *I*: Inclination of mean direction, positive down, $\alpha 95$: width of radius of 95% confidence circle of Fisher mean direction, *k*: Fisher precision parameter.

(a)

Sample	Distance from dike (m)
KP3-1	0.4
KP3-2	0.64
KP3-3	1.71
KP3-4	1.71
KP3-5	~2
KP3-6	~4
KP3-40 to KP3-45	~40-50

(b)

			Geographic coordinates			Tilt-corrected coordinates			
		N	*D* (°)	*I* (°)	$\alpha 95$ (°)	*D* (°)	*I* (°)	$\alpha 95$ (°)	*k*
Dike	HTd	6	319.7	58.9	5.8	16.8	26.5	5.8	6
	LTd	6	1.1	43.8	12.4	17.8	-2.8	12.5	6
Baked samples (KP3-1 to KP3-4)	HTd	10	301.3	63	3.7	20.2	36.2	4.6	10
Unbaked samples (KP3-40 to KP3-45)	HT	12	7.4	44.9	16.2	23.1	-12.6	16.1	7.5
	LT	7	23.2	40.4	30.9	16.7	-2.8	33.4	7

4.0 Discussion

4.1 Discussion and Implications of the baked contact test

The HT components from sites KP1, KP2, and KP4 (Table 1), as well as HT components for KP3 samples far from dike (Table 2b), differ significantly from the HTd components of the dike and baked samples (Table 2b). We interpret this result to imply that bedrock HT components predate dike formation.

It is important to determine whether the dike intrusion predates or postdates the tilt of the bedding into which it intruded. Our logic proceeds as follows:

(1) We have already determined that the bedrock HT component predates dike formation.

(2) If the dike pre-dates the bedding tilting, then the bedrock HT components, because they predate the dike, also predate bedding tilt. Therefore, the bedrock HT components should be expressed in tilt-corrected coordinates.

(3) If the dike post-dates bedding tilting, then the bedrock HT components may or may not pre-date tilting. As it would then be possible that the bedrock HT components formed after bedding tilt, it would be possible that geographic (not tilt-corrected) coordinates are the correct choice for expression of bedrock HT component directions.

We consider the HTd and LTd high-temperature and low-temperature dike magnetization components (Figure 3, Figure A1, Table 1, Table 2b), making the following observations:

(1) The Fisher mean HTd component of the dike samples is offset by ~30° from present-day local field (PLF) in geographic coordinates, implying that this component is likely not recent or is recent but does not average secular variation.

(2) The inclination of the HTd component in tilt-corrected coordinates is intermediate between inclinations predicted by the two double-subduction models of Jagoutz and Royden (2013) and van Hinsbergen et al. (2012).

(3) The Fisher mean LTd component of the dike samples in geographic coordinates is roughly that of the present local field (PLF).

Based on statement (3) we suspect that the LTd dike component constitutes a recent overprint, and based on statements (1-2) we suspect that the dike pre-dates tilting and intruded when the KLA had begun to move to northern latitudes. This northward motion of the KLA occurs after the India-arc collision in Jagoutz and Royden's (2013) model, and prior to any collision in van Hinsbergen et al.'s (2012) model. As the Khardung volcanics are taken to have formed due to tectonic disruption in the region, the baked contact test results favor a scenario of KLA collision followed by northward motion, rather than KLA northward motion followed by collision. Such a scenario is in accordance with the model of Jagoutz and Royden (2013) and disagrees with that of van Hinsbergen et al. (2012). Because we have argued that the dike pre-dated tilting, and because the bedrock HT components have been shown to predate the dike, tilt-corrected coordinates are taken to be the appropriate means for expressing bedrock HT components. Moreover, Fisher mean HT and LT components for sites KP1, KP2, and KP4 have been included for completeness (Figure A1, Table 2b).

4.2 Additional stability arguments

We note in addition that samples from sites KP1-KP4 were unmetamorphosed, and have remained well below 350°C (Jagoutz, Royden, Weiss, personal correspondence). Thus, because remanent magnetization typically persists up to at least ~580°C in our samples, it

is extremely unlikely that complete thermal remagnetization has occurred. Furthermore, persistence of the HT component up to ~580°C indicates the carrier to be magnetite, which is unlikely to have experienced remagnetization from weathering.

4.3 Possible sources of error

We note several possible sources of error in this study. First, is assumed that bedding was horizontal at the time our sampled material was deposited. This assumption is standard in paleomagnetic work. In theory, it would be possible to use the orientation of the dike in relation to the bedding to determine if the bedding was likely horizontal at the time of dike intrusion, because dikes typically form in a vertical orientation; however, in practice, it was difficult to draw any conclusions from this reasoning at site KP3 (Bucholz, personal correspondence). Because present-day bedding strike and dip differ at sites KP1-KP4, consistency of results among sites KP1-KP4 supports the validity of our results.

Two major types of error were present in the sampling process itself. Due to technical difficulties in the field, a majority of cores from sites KP1 and KP3 were not greater than ~5 cm long, yielding only 1 or 2 samples. The short length of these cores led to two types of error in recording their orientation: first, uncertainty when orienting them in the field, and second, excessive play within the clamp guide of the rotating saw used to slice cores into samples, leading to crooked samples. We estimate that the total error for short cores (not greater than ~5 cm) was ~8°, while total error for longer cores was ~5°.

While timing and travel constraints made it impractical to do so, an ideal approach would involved additional samples and sampling sites, as well as spacing sites further apart (on the order of kilometers). Our samples are all within a kilometer of each other, leaving our results susceptible to error from regional effects. Furthermore,

additional samples of bedrock near the dike may have allowed us to observe the components of half-baked samples in addition to the fully remagnetized samples (KP3-1 to KP3-4) and apparently unaffected samples (KP3-40 to KP3-45), which might allow us to better understand the thermal effect of the dike and the rock-magnetic properties at site KP3.

Radiometric dating of our own samples is an important next step. Ar-Ar constraints may also give additional constraints on past heating events. Conglomerate samples were collected from our sites, which may allow a conglomerate test as future work.

Some scatter is evident in the HT components for each site. It is likely that this scatter represents a record of geomagnetic secular variation. Reversals are also seen, indicating that these samples represent at least 10^5 years; therefore, the samples likely represent a long enough timescale that the site mean directions accurately average secular variation (Weiss, personal correspondence). In contrast, a relative lack of scatter, such as is seen in the dike and baked bedrock samples, commonly indicates complete thermal remagnetization. Furthermore, many high-temperature components for samples at site KP4 were not yet origin-trending when the fits were made. When thermal demagnetization of these samples is complete, scatter at site KP4 will likely be reduced.

4.4 At what latitude did the KLA collide with India?

High-temperature (HT) components for bedrock samples from four sites (Tables 1, 2b) were interpreted as constituting the ChRM of these samples. Dike samples and baked KP3 samples (Table 2b) give a significantly different HT component, interpreted to be

the direction at time of dike formation which occurred after that of bedrock formation. Thus, only samples from sites KP1, KP2, KP4 and the unbaked KP3 samples, are believed to give an NRM dating from the time of collision with India. Based on our prior reasoning (Section 4.1), we choose to correct component directions to account for the tilt of the bedding (Figure 4). Tilt-corrected inclinations for HT components at these sites are summarized in Table 3. All four paleolatitudes derived from these inclinations are less than 10° from the equator, with an average of site-mean paleolatitudes of ~5°N. Furthermore, 95% confidence circles for the mean site high-temperature components overlap, meaning plate motion over time cannot be resolved. This likely indicates that material at all sites was emplaced when the volcanics were at roughly the same latitude.

Table 3: Summary of tilt-corrected Inclinations of ChRMs, with corresponding paleolatitudes determined from those inclinations. KP3 (unbaked) refers to samples KP3-40 through KP3-45. Paleolatitudes are sign-corrected to account for geomagnetic reversal.

Site	Component	I (°) [tilt-corrected]	Paleolatitude λ (°N) $\tan I = 2 \tan \lambda$
KP1	HT	-17.4	8.9
KP2	HT	-5.9	3.0
KP3 (unbaked)	HT	-12.6	6.4
KP4	HT	-6.5	3.26

5.0 Conclusions

We have used paleomagnetic sampling and analysis to determine the paleolatitude of samples from the Khardung volcanics of Ladakh at their time of formation. High-temperature components at each of four sites, interpreted to be ChRMs, give roughly

equatorial site mean directions. The average of four paleolatitudes from sites KP1 through KP4 resulting from site mean high-temperature components (Table 3) is ~5°N.

Samples at all sites KP1 through KP4 pass a baked contact test using a dike at site KP3, leading us to conclude that bedrock ChRM predates dike magnetization. The unmetamorphosed nature of our sites and the persistence to high temperatures of the identified HT components precludes complete thermal demagnetization, and persistence to ~580°C indicates magnetite as the likely carrier of these components for the majority of samples.

An equatorial latitude of the KLA at ~50 Ma is in agreement with the double-collision model of Jagoutz and Royden (2013), which has an initial equatorially located collision of India and the KLA at 50 Ma followed by a final continent-continent collision at 40 Ma. Furthermore, our result is tentatively in disagreement with the double-collision model of van Hinsbergen et al. (2012), which gives the KLA an inclination of at least 40° from 60 Ma onward, corresponding to the 25-30°N latitude of the southern margin of Eurasia at the relevant longitude of ~070°E during this time.

References

Allen and Armstrong (2012). Reconciling the Intertropical Convergence Zone, Himalayan/Tibetan tectonics, and the onset of the Asian monsoon system. J. Asian Earth Sci. 44,(30):36-47.

Beaumont, Fullsack, and Hamilton (1992). Erosional control of active compressional orogens. *Thrust Tectonics*, 1992.

Bhutani et al. (2003). Age of the Karakoram fault activation: ^{40}Ar-^{39}Ar geochronological study of Shyok suture zone in northern Ladakh, India. Current Science, 84 (11), (1454-1458)

Bhutani et al. (2009). ^{40}Ar-^{39}Ar dating of volcanic rocks of the Shyok suture zone in north-west trans-Himalaya: Implications for the post-collision evolution of the Shyok Suture Zone. J. Asian Earth Scie. 34, 168-177.

Bouilhol, Jagoutz, Hanchar, and Dudas (2013). Dating the India-Eurasia collision through arc magmatic records. Earth and Planetary Sci. Letters 366:163-175.

Bradley (2013). Segmentation of the Hellenides recorded by Pliocene initiation of clockwise block rotation in Central Grece. Earth and Planetary Sci. Letters 362:6-19.

Cande (2010). Motion between the Indian, Antarctic and African plates in the early Cenozoic. Geophys. J. Int. 183(1), 574.

Cande and Stegman (2011). Indian and African plate motions driven by the push force of the Reunion plume nead. Nature, 475, 47-52

Capitanio et al. (2010) India-Asia convergence driven by the subduction of the Greater Indian continent. (3):136-139.

Dunlap and Wysoczanski (2002). Thermal evidence for early Cretaceous metamorphism in the Shyok suture zone and age of the Khardung volcanic rocks, Ladakh, India. J. Asian Earth Sci. 20 481-490.

Dunlop and Özdemir (1997). Rock Magnetism: Fundamentals and Frontiers (Cambridge Studies in Magnetism).

Gaina, Müller, Brown, Ishihara, Ivanov (2007). Breakup and early seafloor spreading between India and Antarctica. Geophys. J. Int. 170(1):151-169

Jagoutz and Royden (2013, in prep). A Plate Tectonic Explanation for Super Fast Convergence of India and Eurasia.

Jones (2002). User-driven Integrated Software Lives: "PaleoMag" Paleomagnetics Analysis on the Macintosh, Computers and Geosciences, 28 (10), 1145-1151.

Kearey, Klepeis, and Vine. Global Tectonics, Third Edition. Wiley-Blackwell, 306-332.

Khan et al. (2009). Did the Kohistan Ladakh arc collide first with India? GSA Bulletin, 2009. 121:366-384.

Kirschvink (1980). The least-squares line and plane and the analysis of palaeomagnetic data. Geophys. J. Int. 62 (3), 699-718.

Klootwijk et al. (1979). The extent of greater India, II. Palaeomagnetic data from the Ladakh intrusives at Kargil, Northwestern Himalayas. Earth and Planetary Sci. Letters, 44:47-64.

Kumar et al. (2007). The rapid drift of the Indian tectonic plate. Nature 449:894-7.

Molnar (1984). Structure and tectonics of the Himalaya: Constraints and Implications of Geophysical Data. Ann. Rev. Earth Planet. Sci. 12:489-518.

Molnar and England (1990). Late Cenozoic uplift of mountain ranges and global climate change: chicken or egg? Nature, 346:29:34.

Molnar and Tapponnier (1975). Cenozoic Tectonics of Asia: Effects of a Continental Collision. Science 189 (4201): 419-426

Müller, Sdrolias, Gaina, and Roest (2012). Age, spreading rates, and spreading asymmetry of the world's ocean crust. Geochemistry, Geophysics, Geosystem (An AGU Journal). 9(4).

Owen et al. (2002). Climatic and topographic controls on the style and timing of Late Quaternary glaciation throughout Tibet and the Himalaya defined by 10Be cosmogenic radionuclide surface exposure dating. Quaternary Science Reviews, (24:12-13):1391-1411Raymo (1994). The Himalayas, organic carbon burial, and climate in the Miocene. Paleoceanograhy, 9(3):399-404.

Rea (1992). Delivery of Himalayan Sediment to the Northern Indian Ocean and its Relation to Global Climate, Sea Level, Uplift, and Seawater Strontium. Synthesis of Results from Scientific Drilling in the Indian Ocean, American Geophysical Union, 387-402.

Sharma (1978). Potassium argon dating of Dras volcanics, Shyok volcanics and Ladakh granite, Ladakh, northwest Himialaya. Himalayan Geol.

Srimal (1986). India-Asia collision: Implications from the geology of the eastern Karakoram. Geology 14, 523-527.

Tauxe (2010). Essentials of Paleomagnetism. University of California Press.

Thakur and Misra (1984). Tectonic framework of the Indus and Shyok Suture Zones in Eastern Ladakh, Northwest Himalaya. Tectonophysics, 101: 207-220

van Hinsbergen et al. (2011). Acceleration and deceleration of India-Asia convergence since the Cretaceous: roles of mantle plumes and continental collision. J. Geophys. Res 116

van Hinsbergen et al. (2012). Greater India Basin hypothesis and a two-stage Cenozoic collision between India and Asia. PNAS 109 (20): 7659-7664

Yin and Harrison (2000). Geologic evolution of the Himalayan-Tibetan Orogen. Annu. Rev. Earth Planet. Sci. 28:211-80.

Zheng, Powel, Rea, Wang, Wang (2004). Late Miocene and mid-Pliocene enhancement of the East Asian monsoon as viewed from the land and sea. Global and Planetary Change, 41:147-155.

Zhisheng et al. (2001). Evolution of Asian monsoons and phased uplift of the Himalaya-Tibetan plateau since Late Miocene times. Nature 411, 62-66.

Zhu, Kidd, Rowley, Currie, Shafique (2005). Age of initiation of the India-Asia collision in the east-central Himalaya. JSTOR, 113:265-285.

Appendix A – Stereographic plots of mean high-temperature and low-temperature components for sites KP1, KP2, and KP4

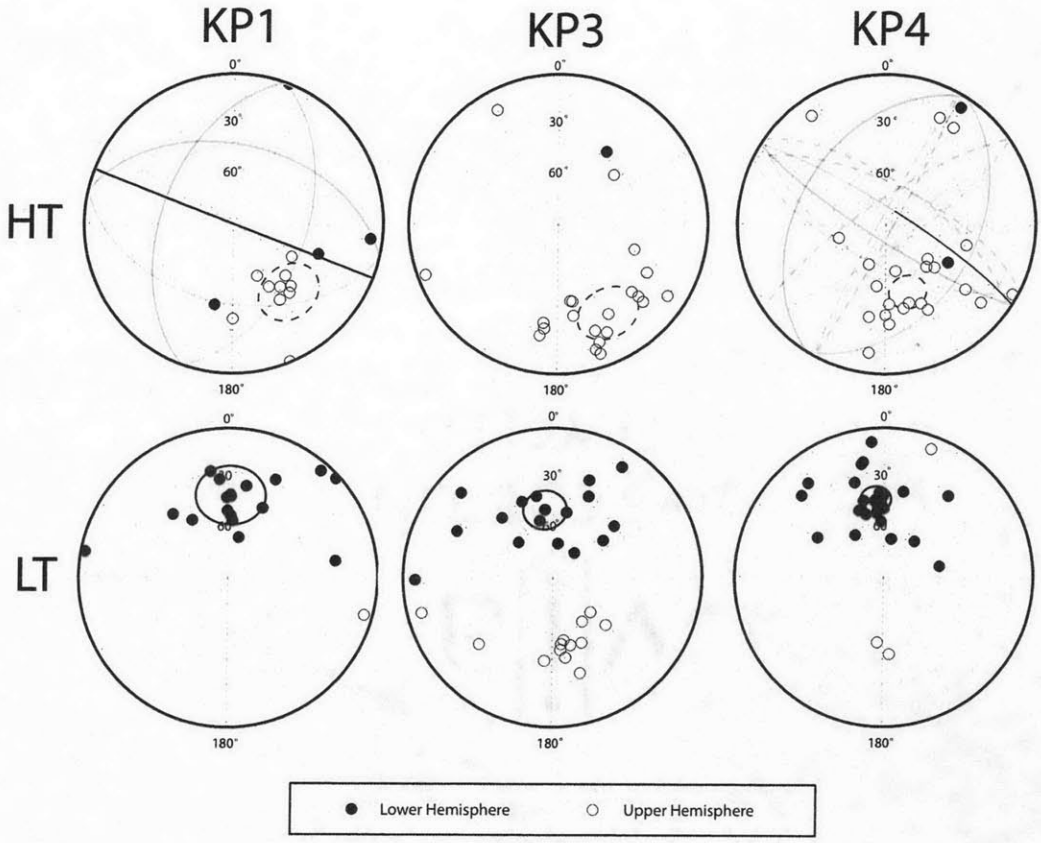

Figure A1: Site mean directions for high-temperature (HT) and Low-temperature (LT) components are given in geographic (non-tilt-corrected) coordinates for sites KP1, KP2, and KP4. Great circles represent best-fit arcs calculated with Fisher statistics, while small circles represent mean site directions.

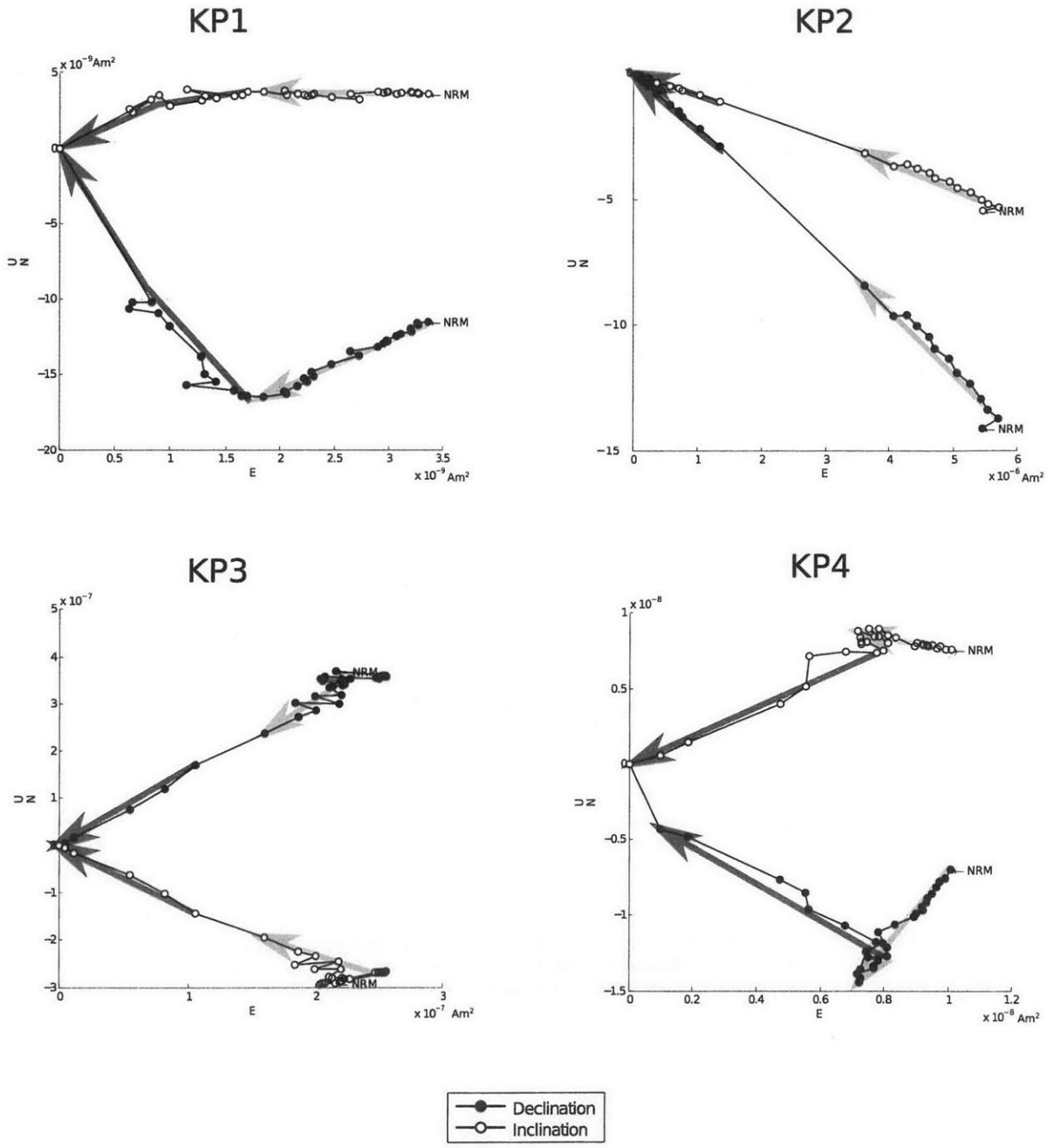

Figure A2: Demagnetization sequences for representative samples from sites KP1-KP4, showing approximate examples of components chosen. Dots represent vector endpoints of magnetization in a north-south orthographic projection. Low-temperature or low-coercivity components are represented with light-grey arrows, while high-temperature components are represented with dark-grey arrows.

Appendix B – Overview of Field Sites

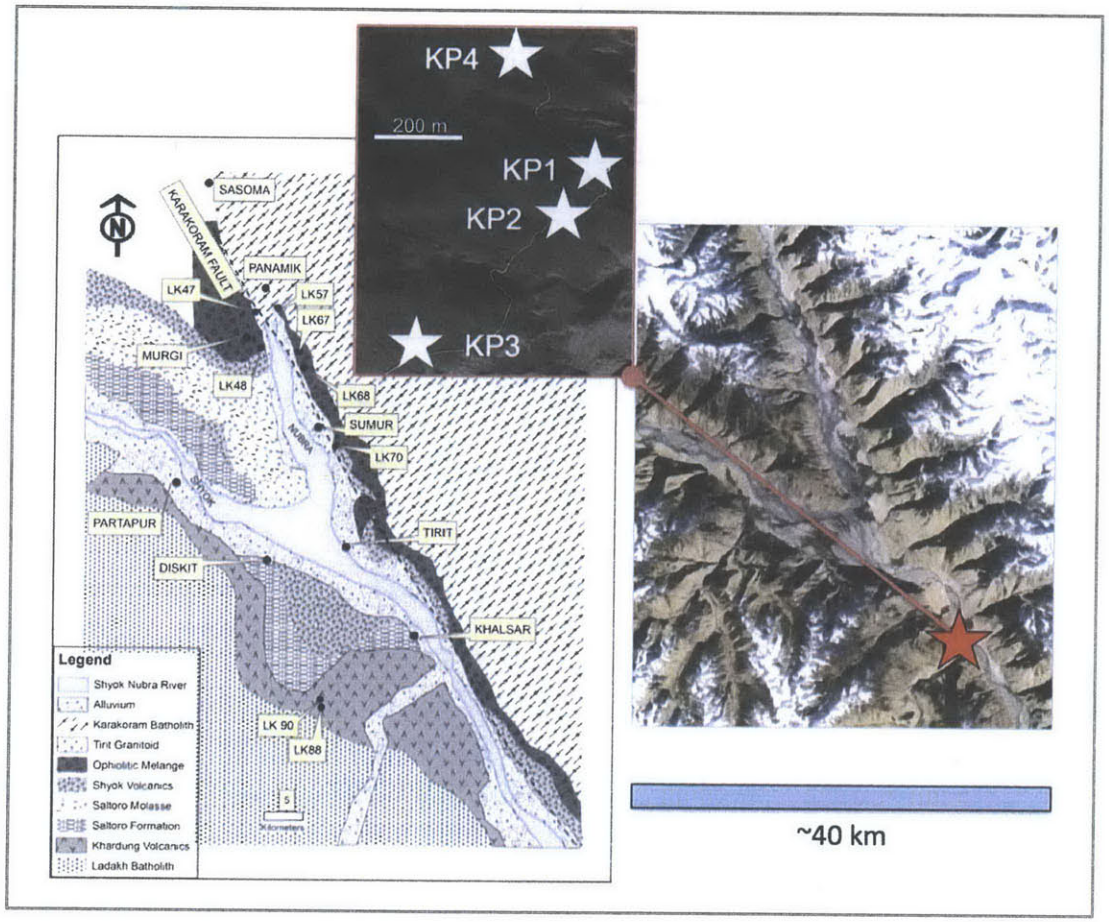

Figure B-1: Local map of field sites. *On left:* figure from Bhutani et al. (2009) showing location of –hardung Volcanic sample sites LK90 and LK88 used for ^{40}Ar-^{39}Ar dating. *On right:* satellite image of region showing locations of our sample sites as stars. The red star represents the location of our 4 sampling sites, which are close enough together to be represented as a single point at that scale. *Inset map:* white stars denote individual sample sites (see Table B-1 for coordinates), thin yellow line represents road.

Table B-1: GPS coordinates of sample sites

Site	Latitude (°N)	Longitude (°E)
KP1	34.4598	077.7230
KP2	34.4530	077.7210
KP3	34.4483	077.7151
KP4	34.4594	077.7189

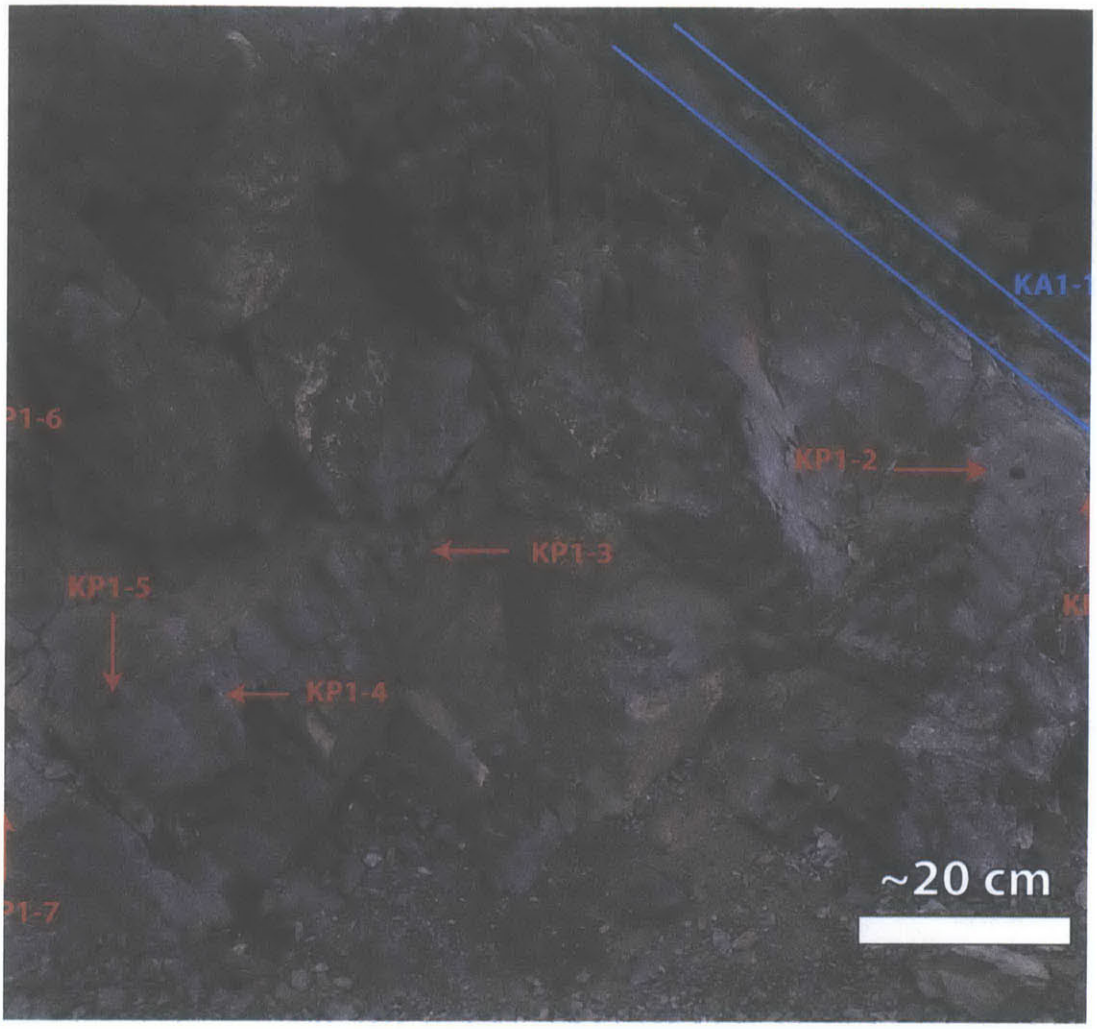

Figure B-2: Photograph of sampling locations at Site KP1 (Image credit: Claire Bucholz)

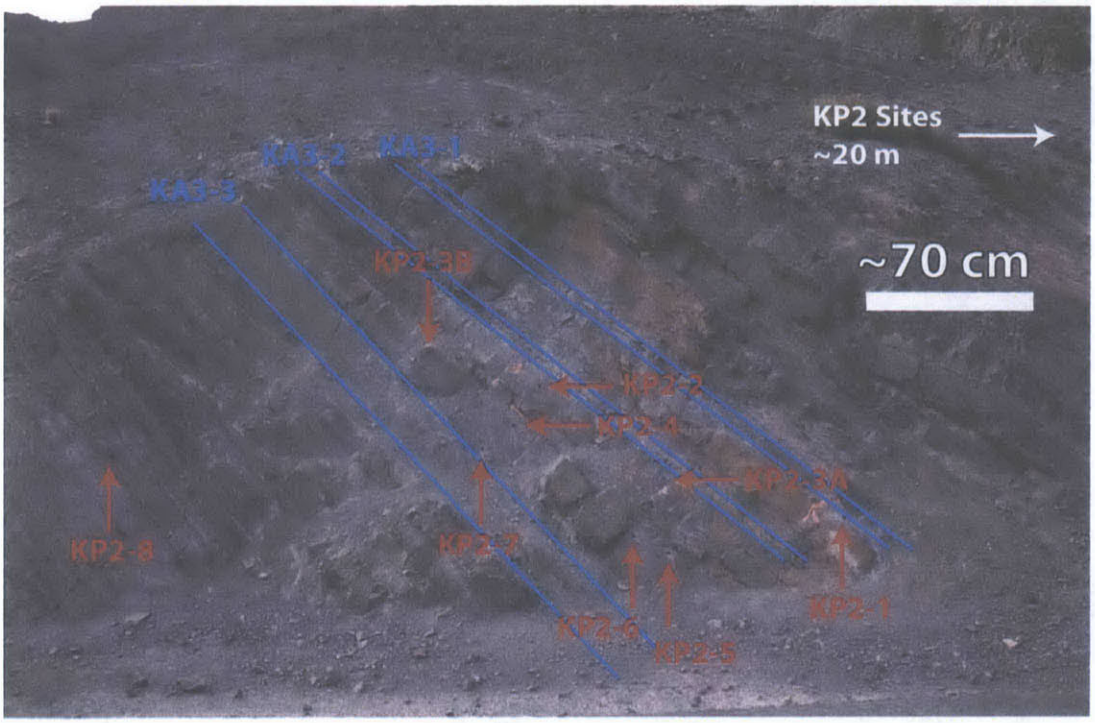

Figure B-3: Photograph of sampling locations at site KP2. KA3-1 through KA3-3 denote ash beds at this site. (Image credit: Claire Bucholz)

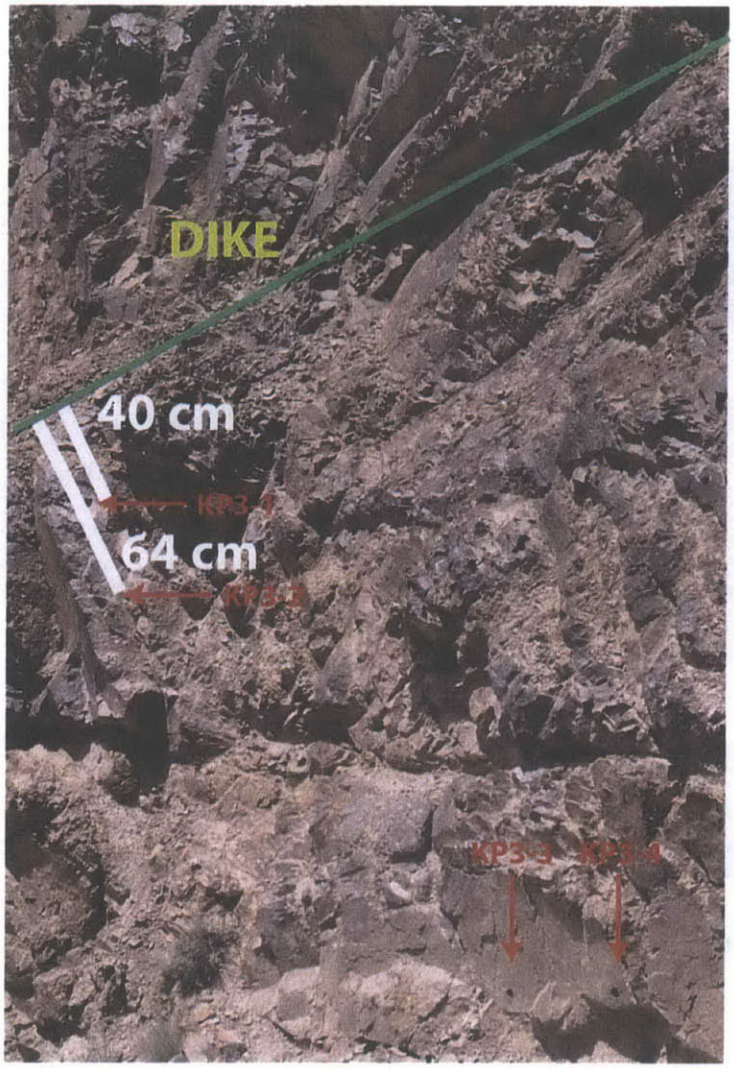

Figure B-4: Photograph of baked sites at KP3. The dike is partially visible at the top of the page, above the green line. (Image credit: Claire Bucholz)

Figure B-5: Photograph of subset of sampling locations at site KP4. (Image credit: Claire Bucholz)